Vacuum-ultraviolet reflectance and photoemission study of the metal-insulator phase transitions in VO_2, V_6O_{13}, and V_2O_3

S. Shin
Research Institute for Scientific Measurements, Tohoku University, 2-1-1 Katahira, Sendai, Miyagi 980, Japan

S. Suga, M. Taniguchi,* M. Fujisawa, and H. Kanzaki†
Synchrotron Radiation Laboratory, Institute for Solid State Physics, The University of Tokyo, 3-2-1 Midori-cho, Tanashi, Tokyo 188, Japan

A. Fujimori and H. Daimon
Department of Physics, Faculty of Sciences, The University of Tokyo, 7-3-1 Hongo, Bunkyo-ku, Tokyo 113, Japan

Y. Ueda,‡ K. Kosuge, and S. Kachi§
Department of Chemistry, Faculty of Science, Kyoto University, Sakyo-ku, Kyoto 606, Japan
(Received 2 August 1989)

Vacuum-ultraviolet reflectance and photoemission spectra of VO_2, V_2O_3, V_6O_{13}, and V_2O_5 are measured in order to investigate the $3d$-band structures and electron-correlation effects. In the case of VO_2, drastic changes in the $3d$ (π^* and $d_\parallel$) -band structures are found in both spectra through the metal-insulator phase transition. The π^* and $d_\parallel$ bands are found at the Fermi level and $E_B=1.3$ eV in the photoemission spectra of metallic VO_2. In the insulating phase, the π^* valence band in the photoemission spectra becomes empty and a rise of the π^* conduction band by about 0.5 eV is found in the reflectance spectra. This band shift through the phase transition may be a driving force of the metal-insulator transition of VO_2. The optical band gap between the $d_\parallel$ valence and π^* conduction bands is obtained as 0.7 eV in the insulating phase, to which the π^*-$d_\parallel$ correlation energy contributes partially. The splitting of the $d_\parallel$ band is also found in the insulating phase. This splitting energy is about 2.5 eV, while the bandwidth of the $d_\parallel$ band is about 1.5 eV. This large band splitting is mainly due to the correlation energy of $d_\parallel$ electrons of about $U(d_\parallel,d_\parallel)=2.1$ eV. On the other hand, no drastic change is found in the $3d$-band structures of V_6O_{13} and V_2O_3 except for slight changes in the bandwidths. Furthermore, the density of states at the Fermi level is rather low in these materials even in the metallic phase. These facts support the view that the electron-correlation effects are important and Mott-type metal-insulator transitions are induced in V_6O_{13} and V_2O_3. Resonant photoemission from V_{3d} and O_{2p} bands are observed as the photon energy is swept through the $3p\rightarrow 3d$ optical-absorption transition. The resonance profiles of V_{3d} bands show the characteristic antiresonance dip, while those of O_{2p} bands show rather broad and simple enhancements. The multiplet structures in the $3p$ core photoemission spectra of VO_2 and V_2O_3 are quantitatively analyzed with use of results from the calculations of Yamaguchi *et al.*

I. INTRODUCTION

It is well known that many compounds may form in the vanadium-oxygen system,[1,2] such as V_2O_3, VO_2, VO, V_2O_5, $V_{2n}O_{5n-2}$ (which is known as the Wadsley phase), and V_nO_{2n-1} (which is known as the Magnéli phase). Most of these materials undergo metal-insulator phase transitions. There have been a lot of experimental and theoretical studies which investigate the mechanism of the metal-insulator transitions.[1,2]

In this work, V_2O_5, V_6O_{13}, VO_2, and V_2O_3 are studied by means of optical and photoemission spectroscopy. The basic properties of these materials are summarized in Table I. V_2O_5 has a layered crystal structure and no $3d$ electrons, and so it is an insulator with a band gap of about 2 eV. V_6O_{13} is a mixed-valence oxide consisting of a $4V^{4+}(d^1)+2V^{5+}(d^0)$ electron configuration showing a metallic conductivity above $T_c=145$ K and becoming insulating below T_c. VO_2 has a $V^{4+}(d^1)$ electron configuration. In the metallic phase above $T_c=340$ K, it has a TiO_2-type crystal structure, while in the insulating phase below T_c, it is distorted to a monoclinic crystal structure. The optical band gap of about 0.7 eV in VO_2 may be the largest of the vanadium oxides which cause metal-insulator transition. V_2O_3 has a $V^{3+}(d^2)$ electron configuration. In the metallic phase above $T_c=168$ K, it has an Al_2O_3-type crystal structure, and a hexagonal crystal structure in the insulating phase below T_c.

In the case of VO_2, it has been considered that the electron-correlation effect is not so evident when compared to the other vanadium oxides. Thus the effect of crystal distortion (or electron-phonon interaction) is thought to be important as a driving force of the metal-insulator transition. Goodenough explained the metal-insulator transition of VO_2 by considering the splitting of the $d_\parallel$ band and the rising of the π^* band within simple crystal-field theory.[3] This also explained the nonmagnet-

 ©1990 The American Physical Society

TABLE I. Basic properties of vanadium oxides V_2O_5, V_6O_{13}, VO_2, and V_2O_3.

	Valence ($3d$ electron number)	Crystal structure	T_c (K)	Transport ($T<T_c$)	Magnetic ($T<T_c$)	Optical band gap
V_2O_5	$V^{5+}(3d^0)$	Orthorhombic (layered)		n-type		~2 eV
V_6O_{13}	$2V^{5+}+4V^{4+}$ ($3d^{0.66}$)	Monoclinic (layered)	145	p-type	Antiferromagnetic ($T_N=55$ K)	?
VO_2	$V^{4+}(3d^1)$	TiO_2 ($T>T_c$) Monoclinic	340	n-type	Nonmagnetic	~0.7 eV
V_2O_3	V^{3+} $(3d^2)$	Al_2O_3 ($T>T_c$) Hexagonal	168	n-type	Antiferromagnetic ($T_N=168$ K)	~0.2 eV

ic properties of VO_2. Gupta, Freeman, and Ellis calculated the electronic band structure in the metallic phase,[4] and concluded that the charge-density waves due to the electron-phonon coupling may be formed in VO_2. The calculation of the lattice dynamics[5] in the metallic phase also suggested that a soft phonon mode exists at the R point of the Brillouin zone. On the other hand, the cluster and band calculation for the insulating phase has shown that the electron correlation is important even in VO_2.

In the case of V_2O_3, it is known that two sorts of overlapping bands, a_{1g} and e_g bands, exist at the Fermi level. Theoretical approaches to the phase transition are usually based on the Hubbard-like Hamiltonian containing these two bands rather than on the change of the band structure alone, since various experimental results[1] show a high correlation of the electrons in V_2O_3. For the mixed-valence compounds, V_nO_{2n-1} (Magnéli phase) and $V_{2n}O_{5n-2}$ (Wadsley phase), it has been considered that the electron-correlation effect is also important, although there are not so many experimental and theoretical studies of these materials, due to their very complicated crystal structure.

In order to know the change in the valence-band structures of vanadium oxides through the metal-insulator transition, a number of photoemission spectra have been measured.[6–14] Changes of the photoemission spectra near the Fermi level (E_F) have been found in some vanadium oxides. However, these changes have not been fully interpreted in connection to the changes in the band structure or electron-correlation effect through the metal-insulator transition.

In addition, a lot of absorption and reflectance spectra have also been measured.[15–23] The spectra have a few broad structures except for the fundamental absorption edge below $h\nu=1$ eV, so it is not easy to discuss the change in the $3d$-band structure in spite of many efforts to do so.

Firstly, we have measured high-resolution vacuum-ultraviolet photoemission spectra of V_2O_5, V_6O_{13}, VO_2, and V_2O_3 using synchrotron radiation, in order to reveal detailed valence-band structures. Next, vacuum-ultraviolet reflectance spectra of these materials were measured in a wide energy range by utilizing the polarization characteristics of synchrotron radiation in order to detect any changes in the conduction band, as well as the valence-band structures. The combination of ultraviolet reflectance and photoemission spectra gives fruitful information about the band structure in connection with the metal-insulator transition.

II. EXPERIMENT

Single crystals of V_2O_5, V_6O_{13}, VO_2, and V_2O_3 were grown by the chemical vapor transport method with $TeCl_4$ as an agent material. The V_2O_5, V_6O_{13}, and V_2O_3 samples had approximate dimensions of $10\times10\times5$ mm^3. VO_2 samples were about $7\times5\times5$ mm^3. V_2O_5 and V_6O_{13} are easily cleaved along the (010) and (001) layers, providing specular surfaces. Specular crystal surfaces of $(110)_r$ and $(111)_r$ are realized in as grown VO_2, though the cleavage provides a $(110)_r$ surface which is not optically smooth (r stands for the rutile structure).

The measurements were performed with synchrotron radiation from a 0.4-GeV electron storage ring (SOR-RING) at the Institute for Solid State Physics, as a light source. For ultraviolet photoemission spectroscopy (UPS), a grazing-incidence monochromator of a modified Rowland-mount type was used to cover the excitation photon energy ($h\nu$) from 30 to 120 eV. The kinetic energy of the photoelectron was analyzed by a double-pass cylindrical mirror analyzer. The overall resolution of the system was around 0.2 eV at $h\nu=30$ eV and 0.25 eV at $h\nu=60$ eV. The base pressure of the sample chamber, as well as the analyzer chamber, was below 2×10^{-10} Torr. The samples of V_2O_5 and V_6O_{13} were cleaved *in situ* at room temperature, providing surfaces parallel to the layer. The samples of VO_2 were cleaved providing $(110)_r$ surfaces. The spectra were measured with $\mathbf{E}\|\mathbf{C}_r$, where $\mathbf{E}$ is the polarization of the incident photon and $\mathbf{C}_r$ is the $\mathbf{C}$ axis in the rutile (metallic) phase. The resonant photoemission spectra of VO_2 were measured for surfaces cleaned by scraping *in situ* with a diamond file. The samples of V_2O_3 were also scraped *in situ* with a diamond file. Photoemission spectra of V_2O_5 were measured only at room temperature. Photoemission spectra of V_6O_{13} and V_2O_3 were measured in the insulating phase at liquid-N_2 temperature and in the metallic phase at room temperature. The spectra of VO_2 were measured in the insulating phase at room temperature and in the metallic phase at 375 K.

For the ultraviolet reflectance spectra, a Seya-Namioka monochromator was used between $h\nu=2$ and 27 eV. In order to reduce the stray light and higher-order light

from the grating, LiF, SiO_2, and glass filters were used. The resolution was set to around 0.008 eV at $h\nu=4$ eV. The measurements were done at an incidence angle of 22.5° with p-polarized light. The reflectance spectra of V_2O_5 and V_6O_{13} were measured on such surfaces as were cleaved in air just before the measurements. The spectra of V_2O_3 were obtained from a natural lusterless crystal surface. The reflectance spectra of VO_2 were measured on natural crystal surfaces of $(110)_r$ and $(111)_r$. For a cleaved $(110)_r$ surface, the reflectance spectra were also measured and confirmed to be the same as for the natural crystal surface. The changes in the spectra on the metal-insulator transition were reproducible.

III. RESULTS

A. Photoemission spectra

1. V_2O_5

Since the $3d$ band is nominally empty in V_2O_5, the valence band consists of mostly O $2p$ bands except for the O $2p$–V $3d$ hybridization due to the bonding effect. The UPS spectrum of V_2O_5, measured at $h\nu=35$ eV, consists of three bands A, B, and C in the binding-energy (E_B) region from 2 to 8 eV, as seen in Fig. 1. The UPS spectrum (solid curve) is very similar to the x-ray photoemission spectroscopy (XPS) spectrum (dotted curve).[24] Both spectra are well explained by the density of states[25] (DOS) obtained by the band calculation. The intensity of the C band is relatively stronger in the XPS spectrum than in the UPS spectrum. This fact shows that the V $3d$ component is more hybridized in the region of the C band than in the other region, since the cross section of the V $3d$ band is larger in XPS.[26]

Figure 2 shows the UPS spectra of the O $2p$ bands for various photon energies. Figure 3 shows the constant-initial-state (CIS) spectra at the position of the three prominent bands, A, B, and C. It is well known that the O $2p$ cross section[26] gradually decreases with photon energies in the present $h\nu$ region, while the V $3d$ cross section resonantly increases at photon energies corresponding to the V $3p$ core excitation. From the observed CIS behavior, the A band at 3.6 eV in the lowest binding-energy region is assigned to the nonbonding O $2p$ band which mainly consists of an O $2p$ component. On the other hand, the band C is assigned to the bonding band hybridized with $3d$ orbitals which contains an appreciable amount of the V $3d$ component, judging from the strong resonance in the photoemission process around the energy region of the V $3p\rightarrow$V $3d$ core excitation, as shown in Fig. 3. The band calculation[25] suggests that the strong bonding σ orbitals exist in the energy region of the structures B and C and the weakly bonding orbitals from the oxygen "lone pair" exist in the energy region of structure A. Thus the CIS spectra are consistent with the band calculation.

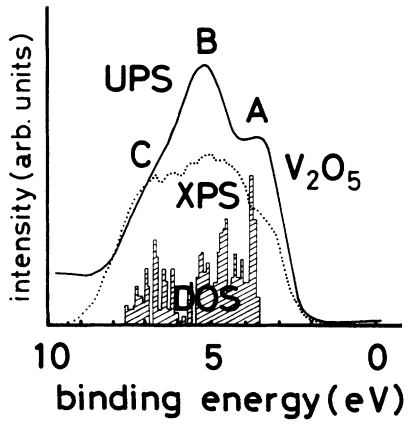

FIG. 1. The solid curve shows the UPS spectrum of V_2O_5 measured at $h\nu=35$ eV. The dotted curve shows the XPS spectrum (Ref. 24). The bar graph shows the density of states (DOS) (Ref. 25).

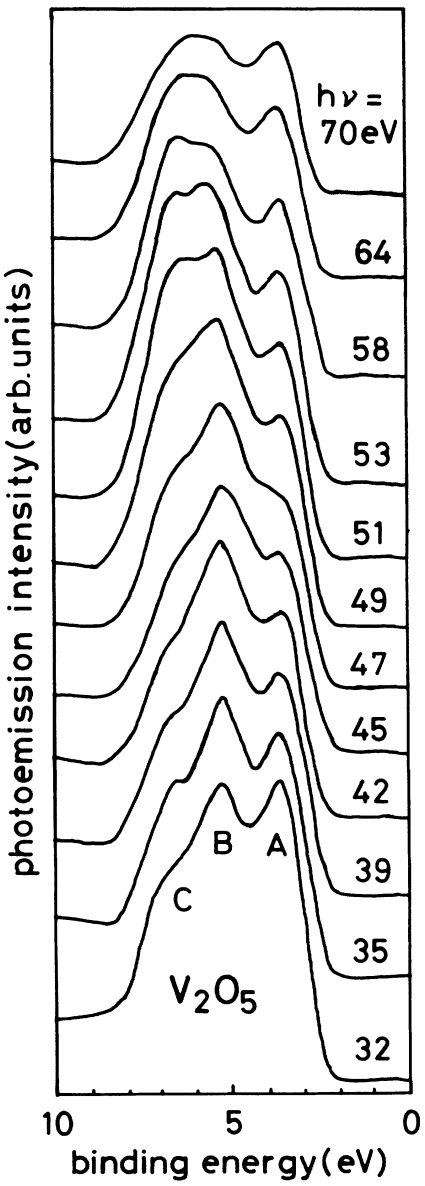

FIG. 2. UPS spectra of V_2O_5 for various photon energies ($h\nu$).

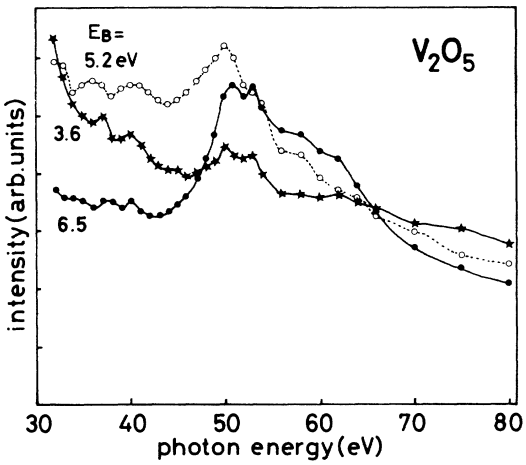

FIG. 3. Constant initial state (CIS) spectra of V_2O_5 at A ($E_B=3.6$ eV), B (5.2 eV), and C bands (6.5 eV).

2. V_6O_{13}

The UPS spectra of V_6O_{13} have O $2p$ band structures consisting of three prominent bands A, B, and C in the energy region from 2 to 8 eV, as shown in Fig. 4. The O $2p$ band in this region is very similar to the O $2p$ band observed in V_2O_5, partly because of the layered crystal structure of V_6O_{13} which is similar to that of V_2O_5. It is found that the O $2p$ bands' intensities change remarkably with excitation energy. Though the detailed excitation energy dependence was not measured, the line shape is very similar to that of V_2O_5 at each $h\nu$. Therefore we consider that the band C is greatly hybridized with the V $3d$ component, while the band A consists almost entirely of the O $2p$ component.

The V $3d$ band is weakly seen in the energy region between 0 and 2 eV. The left panels of Fig. 5 show the $3d$-band spectra in both phases. The maximum of the $3d$ band in the metallic phase (M) is seen around 0.65 eV below the Fermi level (E_F). In the insulating phase (I), the maximum of the $3d$ band is shifted to smaller binding energies by about 0.15 eV, irrespective of band-gap formation at E_F. We have deconvoluted the spectra eliminating the resolution of the system by using the Fourier transformation, as shown in the Appendix. The intensity of the deconvoluted $3d$ band in the insulating phase converges to zero at the Fermi level as shown by the dotted line in Fig. 5. Thus the band gap of V_6O_{13} in the insulating phase is very small. On the other hand, the $3d$ band in the metallic phase shows a noticeable Fermi edge in the deconvoluted spectrum, which is consistent with the metallic conductivity of the $3d$ electrons. A comparison of the deconvoluted spectra shows almost the same energy maximum of the $3d$ band at around 0.5 eV, while the bandwidth decreases by about 0.2 eV on the transition from the metallic to the insulating phase.

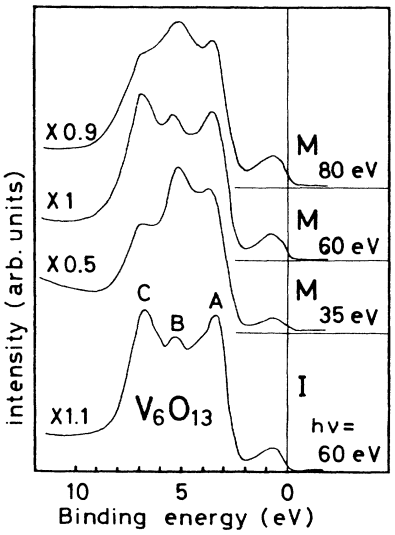

FIG. 4. UPS spectra of V_6O_{13} in the metallic (M) and insulating (I) phases for various $h\nu$. The spectra are shown here by multiplying the factor given in the figure by the calibrated intensity.

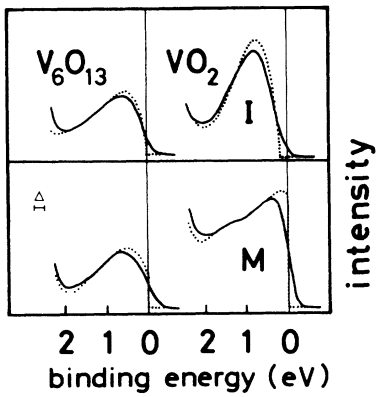

FIG. 5. The solid curves show the UPS spectra of the $3d$ bands of V_6O_{13} and VO_2 in the metallic (M) and insulating (I) phases. The dotted curves show the spectra deconvoluted with the resolution (shown by △).

3. VO_2

Figure 6 shows the UPS spectra of VO_2 for an excitation energy of $h\nu=60$ eV. The solid line shows the spectrum in the insulating phase at room temperature and the dashed line shows it in the metallic phase at 375 K. The O $2p$ band consists of two broad structures, A and B, very different from the three O $2p$ structures in V_6O_{13} and V_2O_5. The $3d$ band is clearly seen in the energy range between 0 and 2 eV. The shape of the $3d$ band drastically changes through the metal-insulator transition, whereas the O $2p$ band shows no noticeable change. One also recognizes a weak structure, C, in the V $3d$ band in the metallic phase. The right-hand panel of Fig. 5 shows the $3d$-band spectra of VO_2. The deconvoluted spectrum of the $3d$ band in the metallic phase shows a clear Fermi edge, as displayed by the dotted line. The maximum of the density of states exists around the Fermi level. This should be compared with the fact that the maximum of the density of states of the $3d$ band of V_6O_{13} is shifted from the Fermi level even in the metallic phase. In the insulating phase of VO_2, however, one clearly notices that

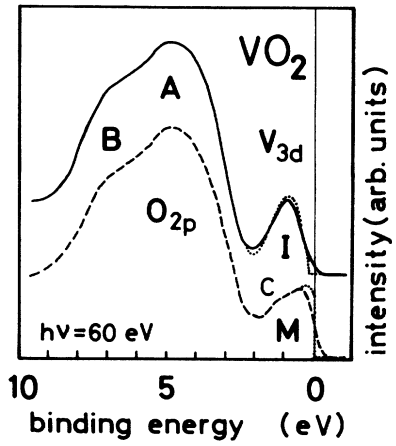

FIG. 6. UPS spectra of VO_2. The solid curve shows the spectrum of the insulating phase measured at 298 K. The dashed curve shows the spectrum of the metallic phase measured at 375 K. The dotted curves show the spectra deconvoluted with the resolution.

the $3d$ band has been shifted considerably from the Fermi level. The band gap of VO_2 in the insulating phase has been already reported in several XPS experiments as 0.3, 0.4, or 0.7 eV,[6-8] although the definition of the band gap was not clear enough. The band gap is defined here as the energy difference between the Fermi level and the top of the valence band probed by means of the photoemission study. For this purpose, high-resolution measurements and the deconvolution of the spectrum are necessary. In the present UPS study, the gap is evaluated as 0.2 eV. In the insulating phase, it is also found that the $3d$ band is a simple band with a maximum of the density of states at around $E_B=0.9$ eV. The $3d$-band width in the insulating phase is evaluated to be about 1.5 eV.

Figure 7 shows the calculated density of states[27] of the valence band compared with the UPS and XPS spectra[6] in the metallic phase of VO_2. The structure near E_F can be well explained by the high density of states due to the

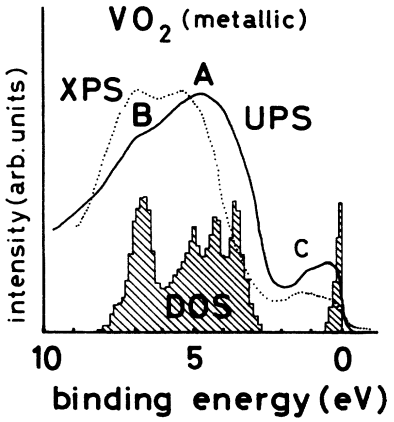

FIG. 7. UPS spectrum (solid curve) of VO_2 in the metallic phase. The dotted curve shows the XPS spectrum (Ref. 6). The hatched spectrum shows the calculated density of states (DOS) (Ref. 27).

V $3d$ band around the Fermi level, as suggested by the band calculation. The line shape of the broad O $2p$ band is also consistent with the band calculation. However, the intensity ratios of the structures, A and B, in the UPS and XPS spectra are remarkably different. Furthermore, the XPS spectrum shows considerable decrease in the intensity around the top of the O $2p$ valence band around $E_B=3$ eV.

Figure 8 shows the UPS spectra in the insulating phase for various photon energies. Figure 9 shows the corresponding CIS spectra of VO_2 at V $3d$ ($E_B=0.9$ eV), A (4.8 eV), and B (7.0 eV) bands compared with the V $3p$ core reflectance spectrum. One can see that the O $2p$ bands (4.8 and 7.0 eV) do not show a remarkable resonance effect in VO_2 in contrast to the strong resonance effect in some part of the O $2p$ band observed in other vanadium oxides. The resonance profile of the O $2p$ bands in VO_2 is indeed broad and the onset of the resonance is recognized around 35 eV with a maximum around 47 eV. For the V $3d$ band (0.9 eV), on the other hand,a weak antiresonance-type dip is recognized in the lower-energy region and the resonance maximum is found around 50 eV. The band calculation[28] of metallic VO_2 suggests that the nonbonding (O $2p\pi$) orbitals exist in the energy region of the A band where the $3d$ component is negligible and the bonding O $2p\sigma$ orbitals exist

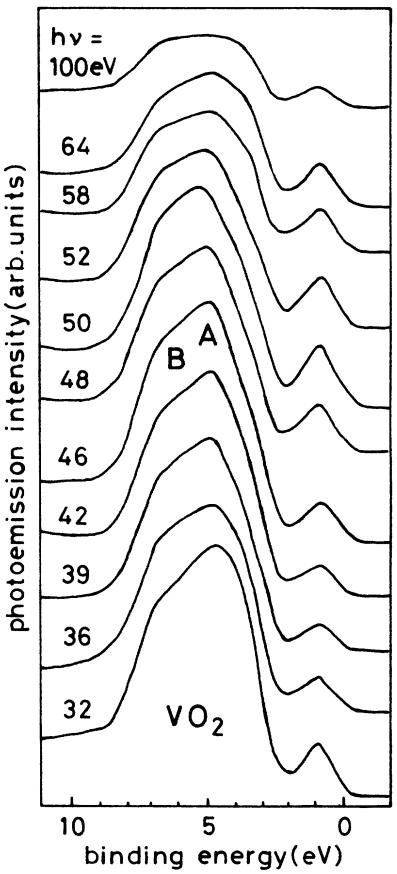

FIG. 8. UPS spectra of VO_2 in the insulating phase for various photon energies.

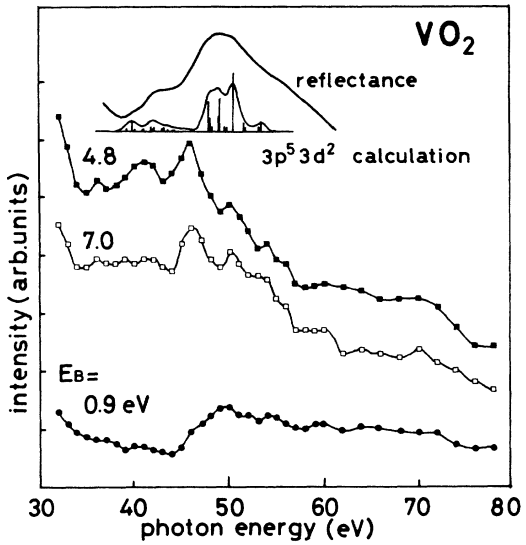

FIG. 9. The reflectance spectrum (Ref. 14) and the constant-initial-state spectra of VO_2 in the insulating phase at V $3d$ ($E_B=0.9$ eV), A (4.8 eV), and B bands (7.0 eV).

in the lowest portion of the O $2p$ band (B band), which consists of strong $3d$ components. The valence levels corresponding to V $3d$–O $2p$ π bonding orbitals are less strongly bound than the O $2p\sigma$ levels overlapping with O $2p\sigma$ levels. That is, bonding π orbitals exist in the energy region around the top of the B band. The CIS spectra at the structure A, however, show similar resonance effects to that of the structure B. This fact suggests that the bonding π orbitals extend to the energy region of the A band, in contrast to the band calculations. On the other hand, the top of the O $2p$ band originates from the nonbonding states as confirmed by the comparison of the XPS and UPS spectra.

4. V_2O_3

Figure 10 shows the UPS spectra of V_2O_3 at $h\nu=60$ eV in both phases. At this $h\nu$ the O $2p$ band mainly consists of two structures, A at $E_B=4.9$ eV and B at $E_B=6.5$ eV. Another structure C at $E_B=7.9$ eV becomes evident for lower excitation photon energies ($h\nu=\sim 39$–47 eV) as seen in Fig. 11. The V $3d$ band of V_2O_3 is strongly seen in the energy range between $E_B=0$ and 3 eV with the peak position around 1.3 eV and a width of around 3 eV. The $3d$-band width in V_2O_3 is the largest of the vanadium oxides we measured. The relative intensity of the $3d$ band, compared to the O $2p$ band, is also the highest, reflecting the $3d^2$ configuration in V_2O_3. The density of states at the Fermi level is very low even in the metallic phase.

The shape of the O $2p$ band shows no appreciable change through the metal-insulator transition, as seen in Fig. 10, whereas the density of states of the $3d$ band at E_F shows a slight increase in the metallic phase. However, no change of the maximum position of the $3d$ band is seen.

Figure 12 shows the CIS spectra of V_2O_3 for several structures. The resonance effect for the $3d$ band is the most prominent among the presently measured vanadium oxides. The resonance effect is also remarkable for the B and C structures (6.5 and 7.9 eV) of the O $2p$ bands. The resonance enhancement of the O $2p$ emission begins at

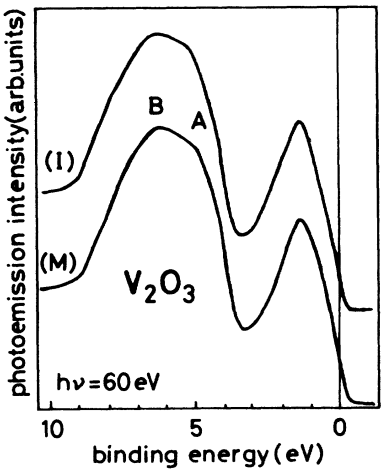

FIG. 10. UPS spectra of V_2O_3 in the metallic (M) and insulating (I) phases.

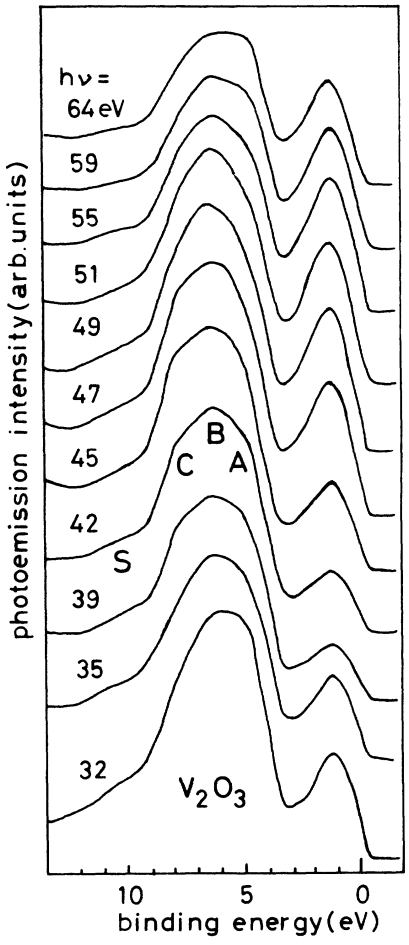

FIG. 11. UPS spectra of V_2O_3 in the metallic phase for various photon energies.

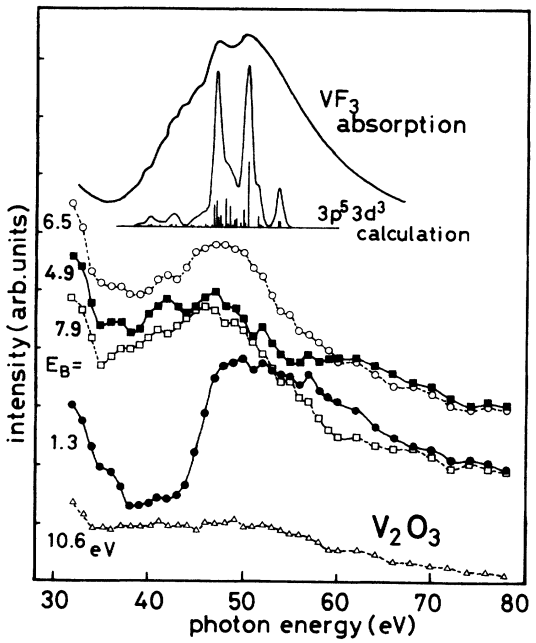

FIG. 12. The corresponding constant-initial-state (CIS) spectra of V_2O_3 at V $3d$ ($E_B=1.3$ eV), A (4.9 eV), B (6.5 eV), C (7.9 eV), and S bands (10.6 eV), which are compared with the absorption spectrum (Ref. 50) of VF_3.

around $h\nu=35$ eV with a maximum at 48 eV. On the other hand, the CIS spectrum of the V $3d$ emission shows a remarkable antiresonance dip in the region of $h\nu=35-45$ eV and a strong enhancement with a maximum around 50 eV.

A weak structure was recently observed around $E_B=10$ eV by Smith and Henrich[12] in the angle integrated UPS spectra of cleaved V_2O_3 and assigned to a satellite structure.[29] Although we have observed a similar structure in the same region, it shows no resonance profile, as seen in the CIS spectra. Therefore its origin is not yet clear.

5. V_{3p} inner core photoemission spectra

The spectra in Fig. 13 show the V $3p$ inner core photoemission spectra of V_2O_3 in both phases for the excitation energy $h\nu=110$ eV. The spectra show three broad structures A, B, and C, which do not change much with the phase transition. The results are consistent with the XPS results obtained by Sawatzky and Post.[8]

Figure 14 shows the V $3p$ inner core photoemission spectrum of VO_2 in the insulating phase at room temperature for the excitation energy $h\nu=110$ eV. The solid lines with the bar graphs in Figs. 13 and 14 are the results of theoretical calculations which will be discussed later.

B. Reflectance spectra

1. V_2O_5

Figures 15 and 16 show the reflectance spectra of V_2O_5. The spectrum is similar to that measured by Mokerov *et al.*[30] The fundamental absorption edge characteristic of an insulator is located at around 2.2 eV. The

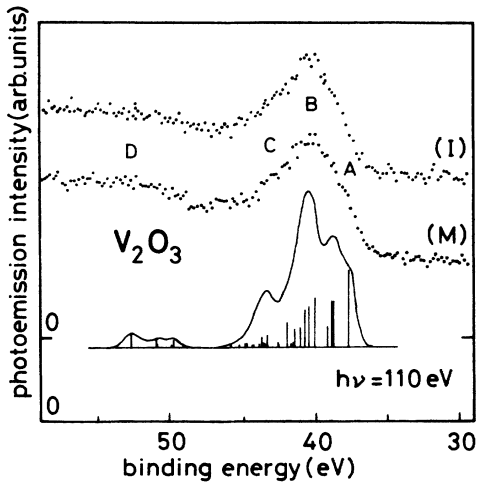

FIG. 13. $3p$ inner core photoemission spectra of V_2O_3 in the metallic and insulating phases. The vertical bars represent the calculated spectrum and the solid line is the spectrum convoluted with a resolution of 1.6 eV (Ref. 53).

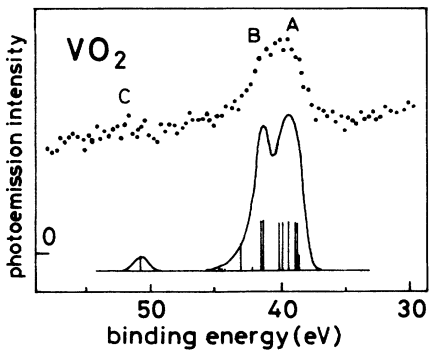

FIG. 14. $3p$ inner core photoemission spectrum of VO_2 at room temperature. The vertical bars are the calculated spectrum and the solid line is the convoluted spectrum (Ref. 53).

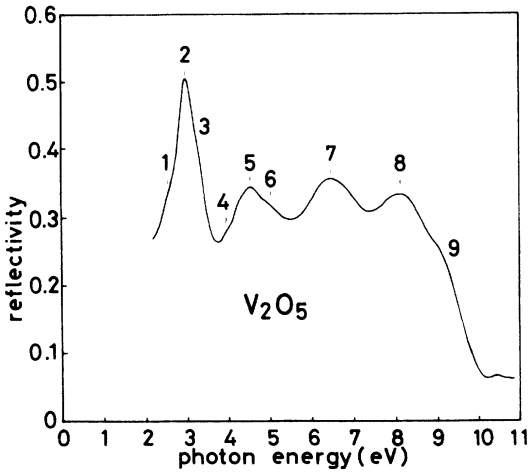

FIG. 15. Ultraviolet reflectance spectrum of V_2O_5 up to $h\nu=11$ eV.

low $h\nu$ spectrum below 10 eV consists of many structures among which the four bands 2, 5, 7, and 8 are prominent. The reflectivity rapidly decreases above 9.5 eV. The structures below this reflectance edge are assigned to the transitions from the O $2p$ valence band to the V $3d$ conduction band, because the O $2p$ band is at the top of the valence band and the V $3d$ band is at the bottom of the conduction band. The peak 2 is rather sharp and can be interpreted as an excitonic transition.

The reflectance spectrum of V_2O_5 in the higher-energy region above 10 eV is shown in Fig. 16. The structures correspond to the transition from the O $2p$ valence band to the V $4s,4p$ higher conduction bands, which exist above the V $3d$ band. The band at around 22 eV may be assigned to the transition from the O $2s$ band to the O $2p$ component hybridized into the V $3d$ band, because the O $2s$ band exists around 21 eV below E_F in the UPS spectra.

2. V_6O_{13}

Figure 17 shows the reflectance spectra of V_6O_{13} in the energy region of the O $2p \rightarrow$ V $3d$ transition above 2 eV. The difference in the reflectance spectra between the metallic and the insulating phases is not clearly discerned. Although the UPS spectra of V_6O_{13} are sharper than those of V_2O_5, the reflectance structures are much broader than those of V_2O_5. The structures numbered 2, 3, 5, and 6 seem to correspond to the bands of 2, 5, 7, and 8 of V_2O_5, respectively. The energy differences of the corresponding bands are within 0.3 eV (most bands in V_6O_{13} are observed at lower energies). No structure is observed around $h\nu=9$ eV in contrast to structure 9 in V_2O_5.

Figure 18 shows the reflectance spectrum in the higher-energy region. The structure at 22 eV is again assigned to the transitions from the O $2s$ to the V $3d$ bands. The other structures for V_6O_{13} correspond to those of V_2O_5, though the energy position of V_6O_{13} is higher by about 0–1 eV. These structures can be assigned to the transitions from the O $2p$ to the V $4s,4p$ bands. However, the line shapes of spectra in this energy region are much broader than those of V_2O_5.

3. VO_2

There have been many experimental studies of the optical spectra of VO_2 in the energy region between 2 and 5 eV.[15–22] Those spectra are subtly different from each other, though bands around 2.8, 3.5, and 4.1 eV are commonly observed in the same energy region. However, the assignments of these bands are not settled yet. In order to check the assignments of these broad band structures, it is useful to measure the spectra with high resolution and by polarization dependence in a wider energy range by using synchrotron radiation as seen below.

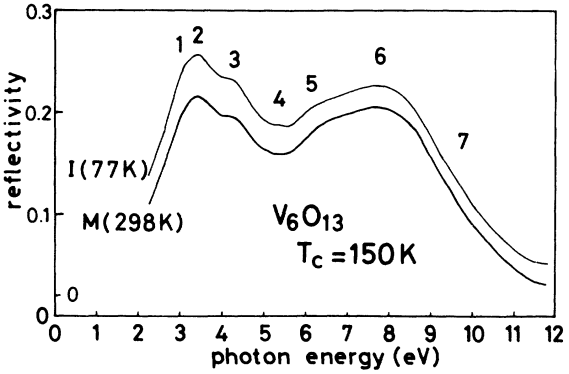

FIG. 17. Ultraviolet reflectance spectra of V_6O_{13} in the metallic (M) and insulating (I) phases, measured at room temperature (298 K) and liquid-nitrogen temperature (77 K), respectively.

Figure 19 shows the reflectance spectra of a natural $(110)_r$ surface of VO_2 measured for the polarization of $\mathbf{E}\|\mathbf{C}_r$. The solid curves (C), (B), and (A) show the spectra in the metllic phase at 375 K, in the insulating phase at room temperature (298 K), and at liquid-N_2 temperature. The dashed curves in the infrared region are the spectra obtained by Dissanayake.[21]

The spectra[21] below 2 eV have shown a reflectance peak associated with the band gap below T_c and the metallic reflectivity (Drude tail) above T_c. The lowest peak in the insulating phase is attributed to the interband transition from the occupied to the empty d bands.

On the other hand, the spectra between 2 and 10 eV are mainly assigned to the transition from the O $2p$ to the V $3d$ bands. Their absorption edge is situated around 2 eV. At liquid-N_2 temperature, the band just above this absorption edge becomes clearer. Although other structures are very broad in both phases, one finds that almost all structures are shifted to higher energies by about 0.5 eV on the transition from the metallic to the insulating

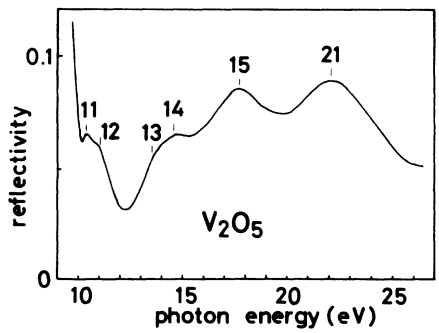

FIG. 16. Ultraviolet reflectance spectrum of V_2O_5 in a region of $h\nu=10$–26 eV.

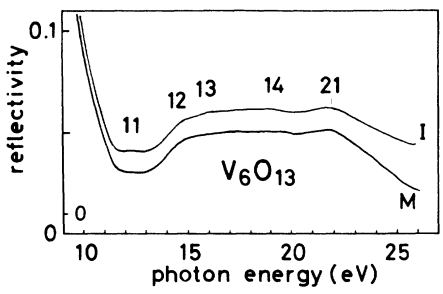

FIG. 18. Ultraviolet reflectance spectra of V_6O_{13} in the metallic and insulating phases. The reflectivity zero is shifted for the spectrum in the insulating phase.

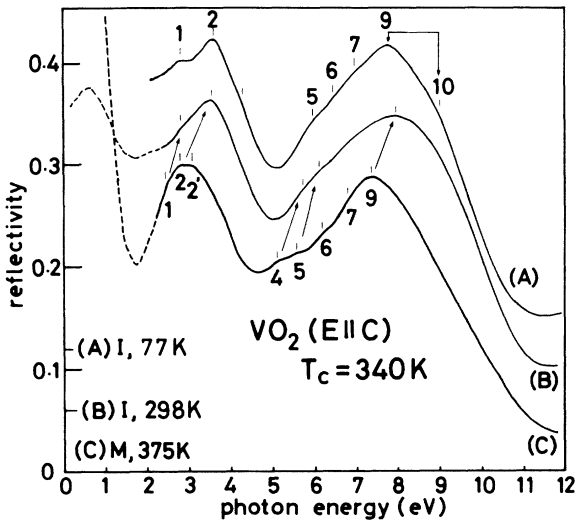

FIG. 19. Ultraviolet reflectance spectra of VO_2 up to 11.5 eV in the metallic (C) and insulating [(A), (B)] phases for the polarization of $\mathbf{E}\|\mathbf{C}$. The spectra of (A), (B), and (C) are measured at liquid-nitrogen temperature, room temperature, and 375 K, respectively, and their reflectivity zeros are shown on the ordinate by (A), (B), and (C). The dashed curves are the reflectance spectra in the infrared light region from Ref. 21.

phase. The shifts of the bands 2, 4, 5, and 9 are especially clear, as indicated by the arrows. The structure 9, around 8 eV, becomes wider in the insulating phase and a shoulder 10 appears around 9 eV. The energy separation between bands 9 and 10 is about 1.1 eV.

Figure 20 shows the reflectance spectra of VO_2 for the polarization of $\mathbf{E}\perp\mathbf{C}_r$ in the same energy region. In the metallic phase, the spectrum is very similar to that measured for $\mathbf{E}\|\mathbf{C}_r$. Therefore we use the same numbers for the corresponding structures. In the insulating phase, a

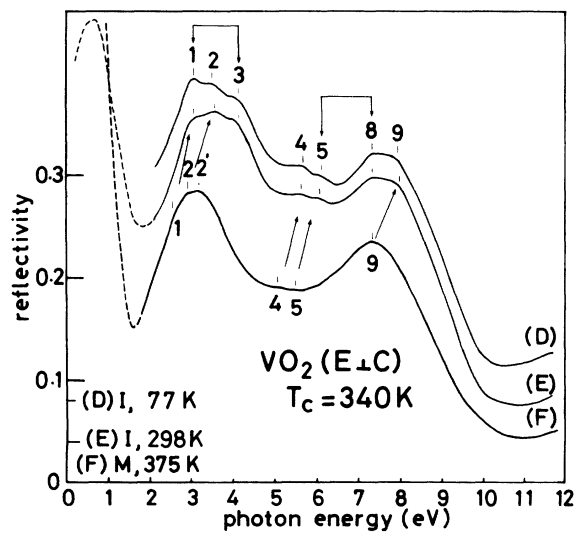

FIG. 20. Ultraviolet reflectance spectra of VO_2 in the metallic (F) and insulating [(D), (E)] phases for the polarization of $\mathbf{E}\perp\mathbf{C}$. The spectra of (D), (E), and (F) are measured at liquid-nitrogen temperature, room temperature, and 375 K, respectively. The dashed curves are the reflectance spectra from Ref. 21.

number of structures shifted to higher energies by about 0.5 eV (structures 1, 2, 4, and 5) are also recognized as in the spectra for $\mathbf{E}\|\mathbf{C}_r$. In this interpretation, however, structure 3 in the insulating phase has no counterpart in the metallic phase. One notices that the energy splitting between structures 1 and 3 in the insulating phase is just 1.1 eV, which is comparable to the splitting between structures 9 and 10 in the insulating phase measured for $\mathbf{E}\|\mathbf{C}_r$. Of the structures 8 and 9 in the insulating phase for $\mathbf{E}\perp\mathbf{C}_r$, band 9 seems to correspond to the band 9 in the metallic phase, because this band 9 shows a similar shift to higher energies by about 0.5 eV in the insulating phase, as does the band 9 for $\mathbf{E}\|\mathbf{C}_r$. In this case, it is not impossible to interpret structure 8 as split from structure 5 in the insulating phase with a mutual splitting of about 1.2 eV. The comparable energy splitting between these structures suggests that they have the same origin induced by the phase transition. As for the polarization dependence of these structures, bands 3 and 8 are only observed in the spectra for $\mathbf{E}\perp\mathbf{C}_r$, whereas band 10 is only observed in the spectra for $\mathbf{E}\|\mathbf{C}_r$.

Figures 21 and 22 show the spectra of VO_2 in the higher-energy region for $\mathbf{E}\|\mathbf{C}_r$ and $\mathbf{E}\perp\mathbf{C}_r$. The reflectance edge due to the exhaustion of the O $2p\rightarrow$V $3d$ transitions is situated at much higher energy for $\mathbf{E}\|\mathbf{C}_r$ (10.5 eV) than for $\mathbf{E}\perp\mathbf{C}_r$ (9.5 eV). The observed structures are mostly assigned to the transitions from the O $2p$ valence bands to the V $4s,4p$ higher conduction bands. It is noticed that several bands (11, 13, 14, 16 for $\mathbf{E}\|\mathbf{C}_r$ and 11 for $\mathbf{E}\perp\mathbf{C}_r$) do not shift much through the metal-insulator transition. On the other hand, the structures above 20 eV, which are assigned to the transitions from the O $2s$ to the V $3d$ bands, shift to higher energies by about 0.5 eV. These facts suggest that the observed energy shifts reflect the shift of the final state of the V $3d$ band on the phase transition, because the band shifts are only seen for O $2p\rightarrow$V $3d$ and O $2s\rightarrow$V $3d$ transitions in contrast to the O $2p\rightarrow$V $4s,4p$ transition. In this sense, the behavior of the reflectance structure 12 and 13 for $\mathbf{E}\perp\mathbf{C}_r$ is rather unusual. It is found that the band 12 appears only in the insulating phase for $\mathbf{E}\perp\mathbf{C}_r$. At the same

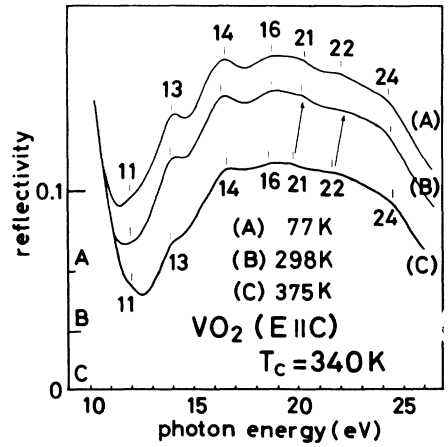

FIG. 21. Ultraviolet reflectance spectra of VO_2 between $h\nu=10.5$ and 26 eV in the metallic (C) and insulating [(A), (B)] phases for the polarization of $\mathbf{E}\|\mathbf{C}$.

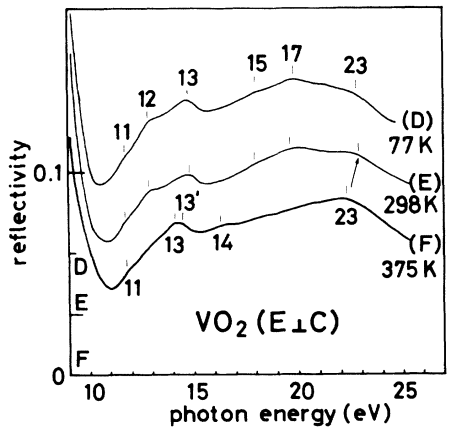

FIG. 22. Ultraviolet reflectance spectra of VO_2 in the metallic (F) and insulating [(D), (E)] phases for the polarization of E⊥C.

time, the peak 13 is shifted to higher energies. It is thus possible that the structures 12 and 13 observed in the insulating phase for $E \perp C_r$ are both derived from the structures 13 and 13' in the metallic phase. This possibility will be discussed later.

The reflectance measurement of VO_2 was performed at various temperatures besides those mentioned above. It is confirmed that the change of the spectra always occurs suddenly at T_c. We have measured many samples including samples cleaved almost parallel to the $(110)_r$ surfaces. The spectral shapes have shown rather strong sample dependence. The spectra given in Figs. 19, 20, 21, and 22 are from a sample which showed the clearest spectral change through the metal-insulator transition.

The changes in the reflectance spectra of VO_2 through the metal-insulator transition are summarized as follows.

(1) Most structures (1, 2, 4, 5, 6, 7, 9, 21, 22, and 23) are shifted to higher energies by about 0.5 eV in the insulating phase.

(2) A few structures (3, 8, 10, and 12) appear only in the insulating phase.

4. V_2O_3

Figures 23 and 24 show the reflectance spectra of V_2O_3 in the metallic phase. The dashed curve in the infrared-light region is the result obtained by Fan.[19] The spectrum below 10 eV mainly consists of four structures. The reflectance structure in the 9–10-eV region is relatively enhanced compared with the results in V_6O_{13} and VO_2. The spectrum above 10 eV of V_2O_3 is very similar to the $E \perp C_r$ spectrum of VO_2, suggesting that the transitions are mostly to the V 4*s*,4*p* bands.

IV. DISCUSSION

A. Assignment of the reflectance spectra

The reflectance spectra of V_2O_5, V_6O_{13}, VO_2, and V_2O_3 are divided into the following four groups.

(1) The reflectance structures below 2 eV are obviously due to the interband transition from the occupied to the

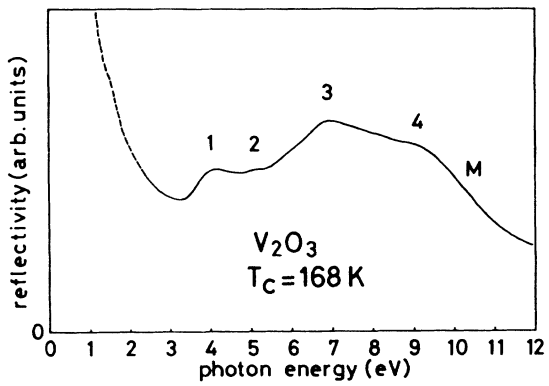

FIG. 23. Ultraviolet reflectance spectrum of V_2O_3 below $h\nu = 12$ eV at room temperature. The dashed curve is the reflectance spectrum in the infrared light region (Ref. 19).

empty 3*d* bands. In the case of V_2O_5, there is no structure in this energy region.

(2) The reflectance spectra between 2 and 10 eV are assigned to transitions from the O 2*p* valence band to the V 3*d* conduction band, because the O 2*p* valence band is observed in the photoemission spectra between $E_B = 2$ and 8 eV. We have summarized in Table II the energy positions of the main reflectance bands (right) and the maximum positions or band edges of the O 2*p* bands revealed by the UPS spectra (left). One can recognize some correspondence between the UPS and the reflectance structures except for certain energy differences between the two values. The peak energies in the reflectance spectra are always higher than the UPS values by about 1, 1, 0.5, and 0.3 eV in V_2O_5, the metallic phases of V_6O_{13}, VO_2, and V_2O_3, respectively. In the case of the insulating phase of VO_2, the energy difference is about 1 eV. These facts suggest that the initial states of these reflectance structures are correlated either with the high density of states of the O 2*p* valence bands or with the edge of the O 2*p* valence band. If we neglect any possible final state interaction, the final states may be within the high density of states of the V 3*d* conduction band about 1, 1, 0.5, and 0.3 eV above the Fermi level in V_2O_5 and the metallic phases of V_6O_{13}, VO_2, and V_2O_3, respectively.

(3) The reflectivity drops rapidly above 10 eV. The spectra between 10 and 20 eV are mostly assigned to transitions from the O 2*p* to V 4*s*,4*p* higher conduction bands. Another possibility is to assign them to the transition from the V 3*d* to V 4*s*,4*p* bands. However, V_2O_5,

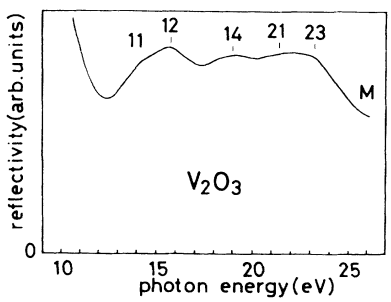

FIG. 24. Ultraviolet reflectance spectra of V_2O_3 between $h\nu = 11$ and 26 eV at room temperature.

TABLE II. Energy positions of the top of the O 2p band and the main structures of the O 2p band in the UPS spectra, which are compared with the main peaks of the reflectance spectra.

V_2O_5		V_6O_{13} (metallic phase)	
UPS	Reflectance	UPS	Reflectance
2.3 eV	→ 3 eV (2)	2.3 eV	→ 3.2 (2)
3.6(A)	→ 4.5 (5)	3.2(A)	→ 4.2 (3)
5.2(B)	→ 6.5 (7)	5.2(B)	→ 6.2 (5)
6.5(C)	→ 8.0 (8)	6.8(C)	→ 7.7 (6)
VO_2 (metallic phase)		V_2O_3 (metallic phase)	
UPS	Reflectance	UPS	Reflectance
2.5 eV	→ 3 eV (1,2)	3.5 eV	→ 4 eV (1)
4.8(A)	→ 5.2 (4,5)	4.9(A)	→ 5.1 (2)
7.0(B)	→ 7.5 (9)	6.5(B)	→ 6.8 (3)
		7.9(C)	→ 9 (4)

with no 3d electron, still shows strong reflectance structures in the above energy region. Therefore the V 3d → V 4s,4p transition does not provide a dominant contribution in this energy region.

(4) Several structures above 20 eV are assigned to transitions from the O 2s to V 3d bands which are hybridized with O 2p orbitals. In the case of VO_2, some structures are also shifted to higher energies in the insulating phase, like the structures observed in the energy region, $h\nu$=2–10 eV. The reflectivity drops gradually above 22–25 eV. The decrease in the reflectivity in this energy region is often called a plasma edge due to the vanishing ϵ_1 and very small ϵ_2 ($\ll 1$).

B. Changes in the band structure of VO_2 through the metal-insulator transition

UPS and reflectance spectra of VO_2 have shown drastic changes in the spectral line shape through the metal-insulator transition, in comparison with other vanadium oxides. The change in the V 3d valence band is detected directly by UPS. The changes in the reflectance spectra are observed in the $h\nu$ region associated with the transitions to the V 3d band from the O 2s or O 2p bands. It is obvious that these changes are caused by changes in the V 3d conduction band.

Goodenough[3] showed that the metal-insulator transition of VO_2 can be explained by changes in the 3d-band structure, considering the crystal structure change. In the metallic phase at higher temperatures, VO_2 has a tetragonal rutile structure, as shown in Fig. 25 (M). The fivefold-degenerate d levels of the $V^{4+}(3d^1)$ ion are first split into doubly degenerate e_g levels and triply degenerate t_{2g} levels in the octahedral crystal field. The e_g orbitals are strongly hybridized with the O 2$p\sigma$ orbitals and have a large bandwidth. The t_{2g} levels are further split into the $d_\parallel$ and π^* levels by the orthorhombic component of the tetragonal crystal field. Thus the $d_\parallel$ and π^* bands are situated at the lowest energies around the Fermi level. Since the π^* orbitals are more hybridized with the O 2$p\pi$ orbitals than the $d_\parallel$ orbitals, the π^* bands have higher energies and a wider bandwidth. On the other hand, the $d_\parallel$ orbitals are rather nonbonding. Thus the $d_\parallel$ and π^* bands overlap at the Fermi level as shown in the schematic diagram in Fig. 26.

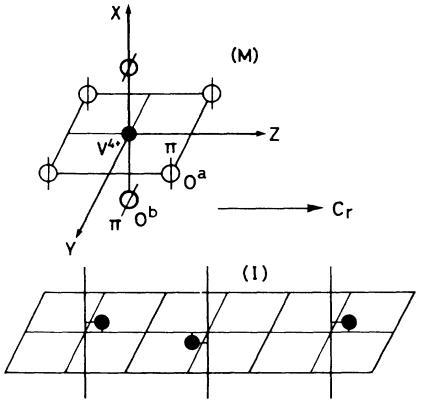

FIG. 25. Tetragonal rutile type crystal structure of VO_2 in the metallic phase (M). In the insulating phase (I), the VO_2 lattice is distorted into the monoclinic crystal structure with the pairing of the vanadium ions.

In the insulating phase, however, VO_2 has a monoclinic structure, where the pairing of the vanadium atoms along the C_r axis occurs as shown in Fig. 25 (I). Because of the change in the V-O hybridization, the energy of the more hybridized π^* band rises above the Fermi level and becomes empty. Furthermore, the $d_\parallel$ band is split into two states by the pairing of the vanadium ions along the C_r axis.

As suggested by Goodenough, the 3d valence band consists of two components in the UPS spectra of metallic VO_2. The high density of states at the Fermi level corresponds to the π^* band and the structure at E_B = 1.3 eV corresponds to the $d_\parallel$ band. In the insulating phase, the π^* band separates from the Fermi level and becomes empty. The UPS spectra in the insulating phase show that the occupied 3d band consists of only a single band ascribable to the lower $d_\parallel$ band, in agreement with Goodenough's suggestion.

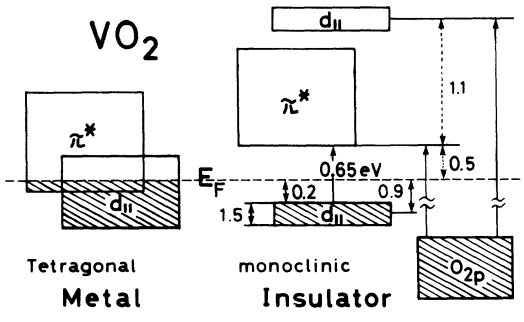

FIG. 26. Schematic energy diagram of the 3d bands around the Fermi level for VO_2. The energy of 0.2 eV is obtained by UPS spectra. The energies of 0.5 and 1.1 eV are obtained by ultraviolet reflectance spectra. 0.65 eV is a value from the infrared absorption spectra (Ref. 15).

With respect to the reflectance spectra, the shift of several structures to higher energies by about 0.5 eV is attributed to the rising of the π^* band, which forms the lowest conduction band. Next, the appearance of several new bands in the insulating phase may be due to band splitting of the $d_{\parallel}$ band. In this case, the energy splitting between the $d_{\parallel}$ and the π^* band is experimentally evaluated to be about 1.1 eV. It is also found in this experiment that transitions to this $d_{\parallel}$ band have an apparent polarization dependence. That is, the bands 3 and 8, which are assigned to the transitions from the top of the O $2p\pi$ band and from the A band (O $2p\pi$) to this $d_{\parallel}$ band, are seen for the polarization $\mathbf{E}\perp\mathbf{C}_r$, as shown in Table III. On the other hand, the band 10, assigned to the transition from the B band (O $2p\sigma$), is seen in the polarization $\mathbf{E}\parallel\mathbf{C}_r$.

Following Goodenough's definition[3] based on the crystal-field theory, where the hybridization effect is not explicitly considered, the wave functions of π^*, $d_{\parallel}$, O $2p\pi$, and O $2p\sigma$ are represented as follows in coordinates with their origin on the V and O atoms, respectively:

$$|\pi^*\rangle=(15/4\pi)XYR_{32}(r),\quad (15/4\pi)ZXR_{32}(r)\ ,$$

$$|d_{\parallel}\rangle=(15/16\pi)(Z^2-Y^2)R_{32}(r)\ ,$$

$$|\mathrm{O}^a\ 2p\pi\rangle=(3/4\pi)XR_{21}(r)\ ,$$

$$|\mathrm{O}^b\ 2p\pi\rangle=(3/4\pi)YR_{21}(r)\ ,$$

$$|\mathrm{O}^a\ 2p\sigma\rangle=(3/4\pi)YR_{21}(r),\quad (3/4\pi)ZR_{21}(r)\ ,$$

$$|\mathrm{O}^b\ 2p\sigma\rangle=(3/4\pi)XR_{21}(r),\quad (3/4\pi)ZR_{21}(r)\ .$$

By calculating the transition moments, $\langle i|\mathbf{e}\mathbf{r}|f\rangle$, it is found that the transition from the O $2p\pi$ to the $d_{\parallel}$ orbitals is forbidden for $\mathbf{E}\parallel\mathbf{C}_r$, while it is allowed for $\mathbf{E}\perp\mathbf{C}_r$. This result is consistent with the experimental polarization dependence of the bands 3 and 8. Furthermore, the calculation for the transition from the O $2p\sigma$ to the $d_{\parallel}$ bands shows that the intensity for $\mathbf{E}\parallel\mathbf{C}_r$ is stronger than for $\mathbf{E}\perp\mathbf{C}_r$. This prediction is also consistent with the experimental polarization dependence of band 10. Because the $d_{\parallel}$ orbital is only weakly hybridized, a calculation done without considering the hybridization will not be a bad approximation for the purpose of qualitative assignment. The components which emerge in the insulating phase with polarization dependence are confirmed to be associated with the transition to the $d_{\parallel}$ band from the O $2p\pi$ and O $2p\sigma$ states. Although the transitions to the e_g band will have strength comparable with the π^* and $d_{\parallel}$ bands, such structures are not resolved in the reflectance spectra due to its broad bandwidth.

TABLE III. Polarization dependence of the reflectance structures of VO_2. These structures are assigned to the transitions from the O $2p\pi$ and O $2p\sigma$ to the $d_{\parallel}$ and the π^* bands.

	$\mathbf{E}\parallel\mathbf{C}_r$	$\mathbf{E}\perp\mathbf{C}_r$
O $2p\pi$ (top; A)$\rightarrow\pi^*$	1,2; 4,5	1,2; 4,5
O $2p\pi$ (top; A)$\rightarrow d_{\parallel}$		3; 8
O $2p\sigma$ (B)$\rightarrow\pi^*$	9	9
O $2p\sigma$ (B)$\rightarrow d_{\parallel}$	10	

The transitions from the O $2s$ state to the π^* band are observed in the energy region beyond $h\nu=20$ eV. However, the transition from the O $2s$ to the $d_{\parallel}$ band cannot be recognized. Since the hybridization with the O $2p$ band is very weak for the $d_{\parallel}$ state compared with the π^* state, the transition from the O $2s$ to the $d_{\parallel}$ band should be much weaker than that to the π^* band.

Among the transitions to the V $4s,4p$ higher conduction bands, band 12 appears only for $\mathbf{E}\perp\mathbf{C}_r$ in the insulating phase, while it cannot be seen in the metallic phase. The V $4s,4p$ higher conduction band may have a rather free-electron-like dispersion curve with $E_k=\hbar^2k^2/2m^*$ in the Brillouin zone, as schematically shown in Fig. 27 (M) for the metallic phase. The structure of the reflectance spectra generally reflects the high joint density of states. The high symmetry points (k_1 or k_2) at the bottom of the conduction band or at the boundary of the Brillouin zone often satisfy such a condition. In the insulating phase, the unit cell becomes doubled along the $\mathbf{C}_r$ axis as shown in Fig. 25 (I) and in Fig. 27 (I). Then a new transition may appear in the insulating phase at the new boundary of the Brillouin zone at $(k_1+k_2)/2$. The band 12, which appears in the insulating phase, is a candidate for such a transition. As detailed band calculations are not available in this energy region, a definite assignment, including the polarization dependence, cannot be given here.

C. Electron correlation effects in VO_2

Based on the above discussion the band structures of VO_2 are summarized in Fig. 26. The splitting energy between the two $d_{\parallel}$ bands is evaluated as

$$2.5=0.9+0.5+1.1\ \text{eV}$$

in the insulating phase, where 0.9 eV is the binding energy of the $d_{\parallel}$ valence band at the maximum, 0.5 eV is the shift of the π^* conduction band, and 1.1 eV is the energy difference between the $d_{\parallel}$ and the π^* conduction bands. The $d_{\parallel}$-band splitting is rather large compared with the

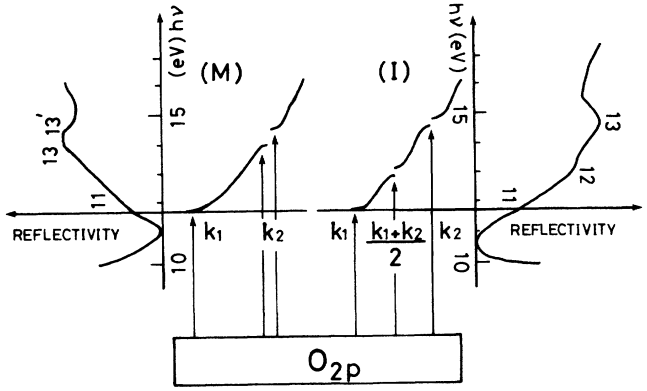

FIG. 27. A possible effect of the crystal distortion on the V $4s,4p$ higher conduction bands in VO_2 through the metal to insulator phase transition. A tentative assignment of the structures of the reflectance spectra to the high symmetry point of the Brillouin zone at k_1 and k_2 in the metallic phase.

$d_{\parallel}$-band width (B) of about 1.5 eV. Since there have been a lot of discussions about the origin of the splitting of the $d_{\parallel}$ bands, we will first consider whether the splitting can be interpreted by the crystal distortion alone. The cluster band calculation[31] showed that the splitting of the $d_{\parallel}$ band is only 0.5 eV in the insulating phase as far as the crystal distortion effect is concerned. Thus the evaluated band splitting ($\sim$2.5 eV) suggests the importance of the electron-correlation energy of the $d_{\parallel}$ electrons. In our experiments, the empty part of the $d_{\parallel}$ band is probed by the electronic transitions from the O $2p$ valence band. The excited $d_{\parallel}$ electron will be subjected to a strong correlation effect with the $d_{\parallel}$ electron staying in the same atom.

Next, we will consider the correlation effect between the $d_{\parallel}$ and the π^* electrons. Figure 28 summarizes various experimental results so far obtained in the insulating phase with respect to the $d_{\parallel}$-π^* band gap. Infrared absorption spectra (C) (Ref. 15) gave a value of about 0.65 eV for the band gap from the top of the $d_{\parallel}$ valence band to the bottom of the π^* conduction band. Electric conductivity measurements have given a value of 0.45 eV for the activation energy.[32,33] Since VO_2 is known as an n-type semiconductor,[34] this activation energy is the energy from the donor level below the Fermi level to the bottom of the π^* conduction band (D). From the reflectance measurement, on the other hand, the shift of the π^* band on the phase transition corresponds to the energy gap between the Fermi level and the bottom of the π^* conduction band in the insulator phase and is evaluated to be 0.5 eV (B). This value is not much different from the result of the conductivity measurements. By means of the UPS measurements in the present experiment, the energy gap between the Fermi level and the top of the $d_{\parallel}$ valence band is evaluated to be 0.2 eV (A). Thus the total band gap, the sum of the two values evaluated by UPS and reflectance spectra, is estimated to be 0.7 eV in good agreement with the results of the infrared absorption spectra.

In the interpretation given in Fig. 26, the Fermi level is situated in the lower part of the band gap. This result seems to be inconsistent with the fact that VO_2 is an n-type semiconductor.[34] This inconsistency may be solved if an electron-correlation energy between the $d_{\parallel}$ and π^* electrons is considered. In the case of the reflectance, infrared absorption, and conductivity measurements, electrons are excited to the π^* conduction band. In these cases, the excited electron can interact with the $d_{\parallel}$ electron. In the case of the UPS measurement, however, the electron-correlation effect between the $d_{\parallel}$ and the excited electron is not so important, because the electron excited to higher conduction bands is rather extended. Thus the value evaluated by the UPS measurement may mainly reflect the band gap due to the crystal distortion. Considering that VO_2 is an n-type semiconductor, the band gap due to the crystal distortion can be estimated from the UPS results to be 0.2–0.4 eV. Thus the energy difference of 0.3–0.5 eV between the above value and the experimentally evaluated band gap (0.7 eV) is interpreted as the electron-correlation energy between the π^* and the $d_{\parallel}$ electrons. In this sense, the correlation energy $U(d_{\parallel},d_{\parallel})$ can be evaluated as 2.1–2.0 eV, subtracting the effect of the crystal distortion from the experimental value of 2.5 eV between two $d_{\parallel}$ bands, where the crystal distortion is taken to be 0.5 eV according to Sommers *et al.*[31] or $\sim$0.4 eV from our UPS results. This value is larger than the theoretical evaluation of the intra-atomic electron-correlation energy of 1.2 eV.[35] The fact that $U(d_{\parallel},d_{\parallel})=2.1$ eV is much larger than the bandwidth, $B=1.5$ eV, indicates that VO_2 is a typical Mott insulator in the low-temperature phase, as has already been suggested by the ESR (Ref. 36) and NMR (Refs. 37 and 38) experiments.

One problem with the band calculation has been that it cannot explain a part of the photoemission line shape of the $3d$ band in metallic VO_2. Namely, the $3d$-band width of the UPS spectra in the metallic phase is much broader than that of the band calculation. In particular, a structure corresponding to the $d_{\parallel}$ band exists around $E_B=1.3$ eV, though the band calculation predicts this $d_{\parallel}$ band just below E_F. The disagreement in the energy position of the $d_{\parallel}$ *band* between the UPS and the band calculation is about 1 eV, reflecting the strong electron-correlation effect of the $d_{\parallel}$ electrons in the metallic phase. The correlation energy of the $d_{\parallel}$ electrons is not negligible even in the metallic phase and $U(d_{\parallel},d_{\parallel})$ is estimated to be not less than 1.3 eV. Thus the $d_{\parallel}$ bands may split into two bands even in the metallic phase, because the $d_{\parallel}$-band width is about 1.5 eV.

There is still a problem as to why the UPS intensity of the π^* band is stronger than that of the $d_{\parallel}$ band in spite of its lower occupation. We consider that the π^* electron is itinerant in the metallic phase and there is a chance that two d electrons can exist on the same vanadium atom at the moment when the itinerant π^* electron comes into the empty $3d$ band. The photoemission from such a configuration ($d^2\rightarrow d^1$) can be observed at smaller binding energies and may overlap with the π^* band. Within the same model, there is a possibility of a d^0 configuration in the metallic phase in accord with the presence of a d^2 configuration. Then the empty state corresponding to the d^0 configuration will have more states

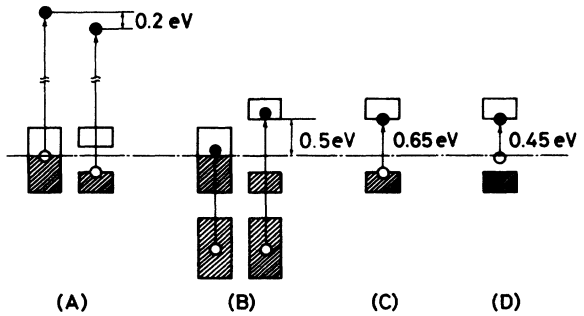

FIG. 28. Estimates of the π^*-$d_{\parallel}$ band gap according to various experimental methods; (A) from UPS measurement, (B) from reflectance measurement, (C) from the infrared absorption measurement (Ref. 15), and (D) from the conductivity measurement (Refs. 32 and 33).

just above E_F in the metallic phase. Thus the reflectance structures of the π^* and $d_{\|}$ bands in the metallic phase become rather obscure because of the overlapping with the d^0 band.

D. The mechanism of the metal-insulator phase transition in VO_2

There have been a lot of discussions regarding the mechanism of the metal-insulator transition in VO_2. In regard to the driving force of the metal-insulator transition, Goodenough[3] first considered the importance of the crystal distortion. Gervais and Kress[5] calculated the phonon dispersion and reported the lattice instabilities at the R point in the Brillouin zone. Gupta *et al.*[4] calculated the electronic band structure in the metallic phase of VO_2 and suggested a charge-density wave (CDW) along the ΓR direction. In fact, the strong electron-phonon interaction has been found by Raman[39] and x-ray[40] experiments in the metallic phase.

In the insulating phase, however, the band splitting of the π^*-$d_{\|}$ and $d_{\|}$-$d_{\|}$ bands cannot be explained by the crystal distortion effect alone, as discussed in the present study. Paquet and Leroux-Hugon[41] have considered both the electron-electron correlation energy and the electron-lattice interaction as the origin of the band splitting. They concluded that the Mott transition is the main origin of the metal-insulator transition, and the crystal distortion is the result.

Zylbersztejn and Mott[32] paid attention to the important role of the π^* electron in the metal-insulator transition. They have thought that the electron-correlation energy is screened by the π^* electron in the metallic phase. In the insulating phase, however, the hybridization between the π^* and the O $2p\pi$ orbitals increases due to the crystal distortion so that the π^* band rises in the energy and becomes empty. Therefore the correlation energy of the $d_{\|}$ electrons becomes enhanced leading to a splitting into the lower and the upper Hubbard bands. As described before, we have observed the rise of the π^* band as well as the splitting of the $d_{\|}$ band into the two bands with a large energy separation. Though the screening effect by the π^* electrons has not been so far discussed quantitatively, we have experimentally concluded that it is a key point for understanding the change in the spectra associated with the metal-insulator transitions in VO_2.

E. Metal-insulator transition of V_2O_3 and V_6O_{13}

The changes in the UPS spectra of V_2O_3 and V_6O_{13} through the metal to insulator transition are very similar. That is, the density of states at E_F is very low even in the metallic phase. Though the $3d$ bands consist of a few bands, they have a single peak at around 1 eV, which does not shift at all through the metal-insulator phase transition. In the insulating phase, the band gaps are not clearly found, because of their small magnitudes. From such UPS results one can recognize the changes in the bandwidths. In this case, the change in the bandwidth is larger in V_6O_{13}.

There have been a lot of studies regarding the metal-insulator transition of V_2O_3. It has been believed[42,43] that the Fermi level exists within the overlapping region of the a_{1g} and the e_π bands and the electronic properties are mainly governed by the e_π electrons. The a_{1g} orbital lies along the **C** axis, while the e_π orbitals are extended perpendicular to the **C** axis. As for the band-structure change of V_2O_3 induced by the crystal distortion,[3] a_{1g} orbitals shift to higher energies due to the lattice expansion along the **C** axis and the a_{1g} state becomes empty. According to the UPS results, however, such a spectral change is not observed. Instead, the a_{1g} state becomes localized according to the expansion of the V-V distance through the metal to insulator phase transition. The e_π electrons also become localized through the exchange interaction J between the a_{1g} and e_π electrons.[42,43] Therefore the slight change in the $3d$ band around E_F in the UPS spectra may reflect such a localization effect of the e_π electrons.

In the case of V_6O_{13}, the mechanism of the metal-insulator transition may be similar to that of V_2O_3, though the band structure is not known. In the case of such mixed-valence materials with complex band structures, the relation between the change in the band structure and the phase transition is not straightforward. The result that the change in the reflectance spectra through the metal-insulator transition is not remarkable suggests that the change in the band structure is also not drastic. It is well known that V-V pairing is formed in the insulating phase for the mixed-valence vanadium oxides.[44] Localization of the $3d$ electrons may also be induced, like the a_{1g} electron in V_2O_3 which provides a smaller bandwidth for the $3d$ band in the insulating phase. Otherwise, the change in the bandwidth may be caused by the change in the V-O distance following the V-V pairing. Such effects will be the main origins of the metal-insulator transition in the mixed-valence compound V_6O_{13}.

F. Resonant photoemission

Recently, there have been reported a lot of theoretical and experimental studies on resonant photoemission from transition-metal compounds. From these studies, new insight into the electronic states has been found for heavy transition-metal compounds. Namely, the strong screening of the $3d$ hole by the charge transfer from anion atoms (that is, $3d^n\underline{L}$ final state where $\underline{L}$ denotes a ligand hole) has been clearly found in the photoemission spectra of the $3d$ transition-metal oxides.[45–48] Such a screening effect is evident for most of the heavy transition-metal compounds. In the case of the light transition-metal compounds, it has been suggested that such a screening effect by charge transfer is small,[46] though there have been very limited numbers of resonant photoemission studies.[12,49] In these experiments, it is said that the photoemission spectral shape of the $3d$ band is very different from that of the heavier transition-metal compounds. The resonance enhancement of the photoemission intensity revealed by the CIS spectra extends over 20 eV for the light transition-metal compounds in contrast to an exten-

sion of about 10 eV for the heavy ones. The energy of the resonance maximum is shifted from the $3p \rightarrow 3d$ threshold by about 10–15 eV, whereas such a shift cannot be found for the heavy ones.

In our resonance experiments of VO_2 and V_2O_3, both the O $2p$ and the V $3d$ bands show resonance enhancement through the $3p \rightarrow 3d$ transition. One notices, however, a clear difference in their resonance profiles. First the V $3d$ band shows a characteristic antiresonance dip around the $3p \rightarrow 3d$ absorption threshold and a remarkable maximum around the absorption maximum at ~ 50 eV. Secondly, the O $2p$ band shows a rather broad profile having some structures around the $3p \rightarrow 3d$ threshold and a maximum at around 48 eV, slightly below the absorption maximum.

One should recall that the CIS spectra of the $3d^n\underline{L}$ final state give an antiresonance dip in heavy transition-metal compounds,[45] whereas those of the $3d^{n-1}$ final state give a simple resonance enhancement without a remarkable antiresonance dip. On the other hand, in the case of vanadium oxides, the CIS spectra of the V $3d$ bands ($3d^{n-1}$ final state) show an antiresonance dip. Moreover, the CIS spectra of the O $2p$ bands do not have an antiresonance dip but give a rather broad and simple enhancement, even though the final state of the photoemission from the O $2p$ band is the same as for the $3d^n\underline{L}$ final state.

Comparing the CIS spectra with the $3p \rightarrow 3d$ absorption spectra, one finds that the CIS spectra of the O $2p$ bands are similar to the absorption spectra. The $3p \rightarrow 3d$ absorption spectra consist of many structures which are well explained by the $3p^5 3d^{n+1}$ multiplet structures[50] with a few dominant structures and some precursor structures below them. In the case of the light transition-metal compounds, the multiplet structures are spread over a wide energy region of about 20 eV which is much larger than in the case of heavy transition-metal compounds. The spectral line shapes of the heavy transition-metal compounds show a typical Fano line shape[50] which is caused by the interference with the background absorption ($3p^6 3d^n \rightarrow 3p^6 3d^{n-1}\epsilon$), because the $3p^6 3d^n \rightarrow 3p^5 3d^{n+1}$ absorption provides the same $3p^6 3d^{n-1}\epsilon$ final state by the super-Coster-Kronig decay. On the other hand, the interference is small in light transition-metal compounds because of the low intensity of the background absorption. Moreover, the spectral line shape is rather broad, in contrast to the asymmetric Fano line shape of heavy transition-metal compounds.

Because the number of occupied $3d$ electrons is smaller in the light transition-metal compounds, the super-Coster-Kronig process may occur less effectively than in the heavy transition-metal compounds. On the other hand, another decay channel is proposed for light transition-metal compounds,[51] as Dehmer *et al.*[52] previously considered for the $4d \rightarrow 4f$ transition of rare-earth elements. The multiplet structures are spread in a wide energy region in the case of light transition-metal compounds, so that some structures at higher energies are situated above the vacuum level. These excited states may interact with the $3p^5 3d^n \epsilon d$ continuum providing the broad line shape. This process would explain the broad line shape of the $3p \rightarrow 3d$ absorption spectra of the light transition-metal compounds. However, these final states cannot directly resonate with the $3d$ photoemission process.

It is noted that some O $2p$ bands of the vanadium oxides show the resonance effect. This fact reveals that the O $2p$ orbitals are partially hybridized with the V $3d$ orbitals in these vanadium oxides. In the case of V_2O_5 and V_2O_3, the hybridization effect is more evident for the deeper energy region of the O $2p$ bands. The O $2p$ band of V_2O_5 at the lowest binding energy ($E_B \sim 3.6$ eV) is less affected by the hybridization effect. In the case of the O $2p$ bands of VO_2, hybridization does not change much through the whole energy region (except for the top of the O $2p$ band). Hybridization is substantial between the O $2p\pi$ and the π^* orbitals as well as between the O $2p\sigma$ and the e_g orbitals. As well, one recognizes that the resonance effect of the V $3d$ band in VO_2 is much less obvious than that of the Ti $3d$ band in Ti_2O_3.[12] This is a surprising fact, because Ti_2O_3 has the same $3d^1$ configuration as VO_2. We think that the more covalent character of VO_2 may be responsible for such behavior. Thus resonant photoemission spectroscopy is a very powerful method to investigate the hybridization effect, though precautions are required for a quantitative discussion.

G. Multiplet structures of V 3p core UPS spectra

The UPS spectra of the V $3p$ core level of V_2O_3 and VO_2 are rather broad as shown in Figs. 13 and 14, suggesting a contribution of multiplet structures. Such structures in V_2O_3 have been also seen in XPS spectra by Sawatzky and Post.[8] Yamaguchi *et al.*[53] calculated the $3p^5 3d^n$ multiplet structures of the $3p$ XPS of transition-metal compounds by taking the $3p$-$3d$ Coulomb and exchange interactions into account, along with the calculation of the $3p^5 3d^{n+1}$ multiplet structures of the $3p$ absorption spectra.[50] The bar graph in Fig. 13 shows the calculated result[53] of the $3p^5 3d^2$ multiplet which is compared with the spectra of V_2O_3. The solid curve shows the calculated spectra with a resolution of 1.6 eV. The parameters of $10Dq = 3.31$ eV and $\kappa_F = 0.7$, $\kappa_G = 0.6$ are used, where κ_F and κ_G are the reduction factors of the Slater-Condon parameters of the $3p$-$3d$ interactions for the free ions. Ordinary values are used for the other parameters such as Racah parameters (B and C), the spin-orbit coupling constant of the $3p$ hole (ζ_{3p}) and Slater-Condon parameters of the free ion (F_2 and $G_{1,3}$), as used in the $3p$ XPS of V^{3+} compounds. The calculated spectrum explains the multiplet splitting of the experimental spectrum well. Here the spread of the multiplet splitting is roughly proportional to the reduction factors which are determined by the covalency between the V $3d$ and the O $2p$ orbitals. The values used for the reduction factors are the same as for the $3p$ core absorption spectra of transition-metal halides[50] which are typical insulators, suggesting that the covalency effect is not so large even in the $3p$ excited state of V_2O_3. Any remarkable change of the multiplet splitting through the metal-insulator transition is not recognized, which shows that the change in the covalency through the metal-insulator transition is

small in V_2O_3.

Figure 14 shows the calculated $3p^5 3d^1$ multiplet structure[53] which is compared with the UPS spectra of VO_2. The parameters, $10Dq = 3.31$ eV and $\kappa_F = 0.7$, $\kappa_G = 0.6$ are used. The other parameters, Racah parameters (B and C), the spin-orbit coupling constant of the $3p$ hole ζ_{3p} and Slater-Condon parameters of free ion (F_2 and $G_{1,3}$) are the same as for the parameters of the $3p$ XPS of Ti^{3+} compounds. The calculated spectrum explains the experimental line shape of VO_2 well, which is much narrower than that of V_2O_3.

V. CONCLUSION

The combination of UPS and reflectance spectra has provided fruitful information about the valence- and conduction-band structures, as well as the electron-correlation effect of $3d$ electrons.

For VO_2, the importance of the itinerant π^* electron for the screening of the $d_\parallel$ electron in the metallic phase is recognized. In the insulating phase, the π^* state rises in energy and becomes empty, because of increased hybridization due to the crystal distortion. Simultaneously, the $d_\parallel$ band splits into two bands. Then the correlation effect for $d_\parallel$ electrons becomes more important. The electron-correlation energy of the $d_\parallel$ electrons and the bandwidth are evaluated to be 2.1 and 1.5 eV in the insulating phase. The band gap between the empty π^* and occupied $d_\parallel$ band is estimated to be 0.7 eV, where the π^*-$d_\parallel$ correlation energy is conjectured to be 0.3–0.5 eV.

In the UPS spectra of V_2O_3 and V_6O_{13}, however, the change in the band structure is not clearly observed except for a slight change in the $3d$-band width. For V_2O_3, the localization of the e_π state may be responsible for the slight change observed in the UPS spectra. For mixed-valence V_6O_{13}, the V-V pairing or the change of the V-O distance may be the cause of the change in the $3d$-band width in the UPS spectra.

The spectral shapes of the $3p$ core photoemission, as well as $3p \rightarrow 3d$ absorption, are quantitatively analyzed based on a ligand field theory.

ACKNOWLEDGMENTS

We are grateful to Professor H. Yasuoka for his useful discussions. The support by the staff of Synchrotron Radiation Laboratory of the Institute for Solid State Physics, The University of Tokyo, is gratefully acknowledged.

APPENDIX

The deconvolutions of the UPS spectra are given as follows, where $f(x)$ is the observed spectra, $f_0(x)$ is the deconvoluted spectra, and $g(x)$ is a Gaussian whose half-width is given by the resolution of the system:

$$F(y) \equiv (2\pi)^{1/2} \int f(x) e^{-ixy}\, dx \ ,$$

$$F_0(y) \equiv (2\pi)^{1/2} \int f_0(x) e^{-ixy}\, dx \ ,$$

$$G(y) \equiv (2\pi)^{1/2} \int g(x) e^{-ixy}\, dx \ ,$$

$$f(x) = \int f_0(t) g(x-t) dt \ ,$$

$$F(y) = (2\pi)^{1/2} F_0(y) G(y) \ ,$$

$$f_0(x) = (2\pi)^{1/2} \int [F(y)/G(y)] e^{-ixy} dy \ .$$

---

*Present address: Department of Material Science, Faculty of Science, Hiroshima University, Hiroshima 730, Japan.

†Present address: Research Laboratories, Fuji Photo Film Co., Ltd. Ashigara, Kanagawa 250-01, Japan.

‡Present address: Institute for Solid State Physics, the University of Tokyo, 7-22-1 Roppongi, Minato-ku, Tokyo 106, Japan.

§Deceased.

[1] N. F. Mott, *Metal-Insulator Transition* (Taylor and Francis, London, 1974).

[2] D. Adler, Rev. Mod. Phys. **40**, 714 (1968).

[3] J. B. Goodenough, J. Solid State Chem. **3**, 490 (1971).

[4] M. Gupta, A. J. Freeman, and D. E. Ellis, Phys. Rev. B **16**, 3338 (1977).

[5] F. Gervais and W. Krèss, Phys. Rev. B **31**, 4809 (1985).

[6] G. K. Wertheim, M. Campagna, H. J. Guggenheim, J. P. Remeika, and D. N. E. Buchanan, in *Magnetism and Magnetic Materials—1974*, edited by C. D. Graham, Jr., G. H. Lander, and J. J. Rhyne (AIP, New York, 1975), p. 235.

[7] C. Blaauw, F. Lennhouts, F. Van der Woude, and G. A. Sawatzky, J. Phys. C **8**, 459 (1975).

[8] G. A. Sawatzky and D. Post, Phys. Rev. B **20**, 1546 (1979).

[9] R. J. Powell, C. N. Berglund, and W. E. Spicer, Phys. Rev. **178**, 1410 (1969).

[10] N. Beatham, I. L. Fragala, A. F. Orchard, and G. Thornton, J. Chem. Soc. Faraday Trans. 2 **76**, 929 (1980).

[11] S. Vasudevan, M. S. Hegde, and C. N R. Rao, Solid State Commun. **27**, 131 (1978).

[12] K. E. Smith and V. E. Henrich, Phys. Rev. B **38**, 9571 (1988).

[13] K. E. Smith and V. E. Henrich, Phys. Rev. B **38**, 5965 (1988).

[14] S. Shin, S. Suga, M. Taniguchi, M. Seki, H. Kanzaki, Y. Ueda, K. Kosuge, and S. Kachi (unpublished).

[15] L. Ladd and W. Paul, Solid State Commun. **7**, 425 (1969).

[16] H. W. Verleur, A. S. Barker, and C. N. Berglund, Phys. Rev. **172**, 788 (1968).

[17] V. G. Mokerov and A. V. Rakov, Fiz. Tverd. Tela (Leningrad) **11**, 197 (1969) [Sov. Phys.—Solid State **11**, 150 (1969)].

[18] G. F. Derbenwick, Ph.D. thesis, Stanford University, 1970.

[19] J. C. C. Fan, Ph.D. thesis, Harvard University, 1972.

[20] A. Gavini and C. C. Y. Kwan, Phys. Rev. B **5**, 3138 (1972).

[21] M. A. K. L. Dissanayake, Ph.D. thesis, Indiana University, 1977.

[22] A. Bianconi, S. Stizza, and R. Bernardini, Phys. Rev. B **24**, 4406 (1981).

[23] P. Shuker and Y. Yacoby, Phys. Rev. B **14**, 2211 (1976).

[24] L. Fiermans, R. Hoogewijs, and J. Vennik, Surf. Sci. **47**, 1 (1975).

[25] W. Lamberrecht, B. Djafari-Rouhani, M. Lannoo, and J. Vennik, J. Phys. C **13**, 2485 (1980); L. Fiermans, P. Clauws, W. Lambrecht, L. Vandenbroucke, and J. Vennik, Phys. Status Solidi A **59**, 485 (1980).

[26] J. J. Yeh and I. Lindau, At. Data Nucl. Data Tables **32**, 28

(1985).
[27]E. Caruthers, L. Kleimmann, and H. I. Zhang, Phys. Rev. B **7**, 3753 (1973).
[28]M. Gupta and D. E. Ellis, Phys. Rev. B **13**, 3405 (1976).
[29]D. K. G. de Boer, C. Haas, and G. A. Sawatzky, Phys. Rev. B **29**, 4401 (1984).
[30]V. G. Mokerov, V. L. Mokerov, V. B. Tulvinsky, and A. R. Begishev, Opt. Spectrosc. **40**, 104 (1976).
[31]C. Sommers, R. DE. Groot, D. Kaplan, and A. Zylberstein, J. Phys. (Paris) Lett. **36**, L157 (1975).
[32]A. Zylbersztejn and N. F. Mott, Phys. Rev. B **11**, 4383 (1975).
[33]J. Molenda and A. Stoklosa, Solid State Ionics **36**, 43 (1989).
[34]W. H. Rosevear and W. Paul, Phys. Rev. B **7**, 2109 (1972).
[35]C. Sommers and S. Doniach, Solid State Commun. **28**, 133 (1978).
[36]J. P. D'Haenen, D. Kaplan, and P. Meranda, J. Phys. C **8**, 2267 (1975).
[37]J. P. Pouget, H. Launois, T. M. Rice, P. Dernier, A. Gossard, G. Villeuve, and P. Hagenmuller, Phys. Rev. B **10**, 1801 (1974).
[38]K. Takanashi, H. Yasuoka, Y. Ueda, and K. Kosuge, J. Phys. Soc. Jpn. **52**, 3953 (1983).
[39]R. Srivastava and L. L. Chase, Phys. Rev. Lett. **27**, 727 (1971).
[40]D. B. McWhan, M. Marezio, J. P. Remeika, and P. D. Dernier, Phys. Rev. B **10**, 490 (1974).
[41]D. Paquet and P. Leroux-Hugon, Phys. Rev. B **22**, 5284 (1980).
[42]J. Ashkenazi and M. Weger, Adv. Phys. **22**, 207 (1973); J. Phys. (Paris) Colloq. **37**, C4-189 (1976).
[43]C. Castellani, C. R. Natori, and J. Ranninger, Phys. Rev. B **18**, 4945 (1978); **18**, 4967 (1978); **18**, 5001 (1978).
[44]A. C. Gossard, F. J. Di Salvo, L. C. Erich, J. P. Remeika, H. Yasuoka, K. Kosuge, and S. Kachi, Phys. Rev. B **10**, 4178 (1974).
[45]A. Fujimori and F. Minami, Phys. Rev. B **30**, 957 (1984).
[46]G. A. Sawatzky and J. W. Allen, Phys. Rev. Lett. **53**, 2339 (1984).
[47]A. Fujimori, M. Saeki, N. Kimizuka, M. Taniguchi, and S. Suga, Phys. Rev. B **34**, 7318 (1986).
[48]L. C. Davis, J. Appl. Phys. **59**, R25 (1986).
[49]J. Berth, R. Stochbauer, and T. E. Madey, Phys. Rev. B **27**, 1939 (1983); Surf. Sci. **141**, 355 (1984); R. D. Bringans and H. Hochst, Phys. Rev. B **30**, 5416 (1984); Y. Ueda, H. Negishi, M. Koyano, M. Inoue, K. Soda, H. Sakamoto, and S. Suga, Solid State Commun. **57**, 839 (1986); P. A. P. Lindberg, L. I. Johansson, J. B. Lindstrom, and D. S. L. Law, Phys. Rev. B **36**, 939 (1987); J. Lindstrom, P. A. P. Lindberg, L. I. Johansson, D. S. L. Law, and A. N. Christensen, *ibid.* **36**, 9514 (1987).
[50]T. Yamaguchi, S. Shibuya, S. Suga, and S. Shin, J. Phys. C **15**, 2641 (1982); S. Shin, S. Suga, M. Taniguchi, H. Kanzaki, S. Shibuya, and T. Yamaguchi, J. Phys. Soc. Jpn. **51**, 906 (1982).
[51]E. Bertel, R. Stochbauer, and C. Kunz, Phys. Rev. B **31**, 2022 (1985).
[52]J. L. Dehmer, A. F. Strace, U. Fano, J. Suger, and J. W. Cooper, Phys. Rev. Lett. **26**, 1521 (1971); J. Suger, Phys. Rev. B **5**, 1785 (1972).
[53]T. Yamaguchi, S. Shibuya, and S. Sugano, J. Phys. C **15**, 2625 (1982); T. Yamaguchi, S. Shibuya, and S. Sugano, The Institute for Solid State Physics, The University of Tokyo Technical Report No. A1159, 1981 (unpublished).